European Polymer Journal 219 (2024) 113328

Contents lists available at ScienceDirect

European Polymer Journal

journal homepage: www.elsevier.com/locate/europolj

Synthesis, characterization and antitumor activity of a *poly*-4-Vinyl pyridine-co-cannabidiol polymer

David Fuentes-Ríos [a], Federico Moya-Utrera [a], Javier Moreno [b,c], Cristina Mesas [b,c], Manuel Doña-Flores [a], Francisco Sarabia [a], J. Manuel López-Romero [a,*], Consolación Melguizo [b,c,d], José Prados [b,c,d]

[a] Department of Organic Chemistry, Faculty of Sciences, University of Málaga, 29071 Málaga, Spain
[b] Institute of Biopathology and Regenerative Medicine (IBIMER), Center of Biomedical Research (CIBM), University of Granada, 18100 Granada, Spain
[c] Instituto de Investigación Biosanitaria ibs. Granada, 18012 Granada, Spain
[d] Department of Anatomy and Embryology, Faculty of Medicine, University of Granada, 18071 Granada, Spain

ARTICLE INFO

Keywords:
CBD co-polymer
CBD solubility
Lung cancer
Polymeric drug

ABSTRACT

Due to its natural origin and numerous beneficial properties, cannabidiol (CBD), one of the major phytocannabinoids of the *Cannabis sativa* L., has attracted the attention of many research groups in recent years. In this work, we prepared 4-vinylpyridine (4VP) and CBD co-polymeric nanoparticles (solid@*poly*-4VP-co-CBD) using *N,N'*-methylenbisacrylamide (BIS) as cross-linker, and in which CBD is covalently incorporated into the polymeric structure. We evaluated particle morphology by Transmission Electron Microscopy (TEM), while compositional analyses were carried out by Nuclear Magnetic Resonance (NMR) spectroscopy, MALDI mass spectrometry, and Raman and Energy Dispersive X-Ray (EDX) spectroscopies. Moreover, the antitumor effect was analyzed in A549 human lung cell lines, using cell cycle analysis and antiproliferative assays. Interestingly, the polymeric drug retained the cytotoxic and antiproliferative effects of CBD. This fact shows that the solid@*poly*-4VP-co-CBD system can be considered as a new polymeric drug (PD) and may have an enormous potential since it can make up for the shortcomings of the use of free drugs such as low stability or bioavailability.

1. Introduction

Over the last years, there have been an increasing interest in *Cannabis sativa* L. chemical constituents, mainly on the non-psychoactive counterparts. Particularly, cannabidiol (CBD) has elicited special interest as one of the most important cannabinoids due to its broad therapeutic activities reported [1–3], including anti-inflammatory, immunosuppressive, antipsychotic, anxiolytic, antiepileptic, antiemetic, antioxidant, anticonvulsant or hypotensive properties. Additionally, it has been reported that CBD is well tolerated by the patient with little secondary effects along a wide range of doses [3–7]. CBD is already used for the treatment of neurodegenerative illnesses like epilepsy, Parkinson, or Alzheimer [2,5], and combined with temozolomide in preclinical therapy against glioma [8]. In addition, there is currently great interest in CBD as an antitumor compound due to its ability to activate cell apoptosis, modify cancer stem cells and reduce the rate of proliferation, angiogenesis, migration and inflammation by influencing cells signaling pathways in numerous types of cancer, including lung cancer [9–11]. However, therapeutic application of CBD is strongly limited, mainly due to its poor foaming, low solubility and bioavailability, high sensitivity to environmental conditions, and poor emulsifying properties in water at neutral pH and in hydrophilic solvents [12,13].

Consequently, many efforts have been devoted to improving CBD properties, especially solubility, and to provide a controlled release. To this aim, various delivery systems have been designed and developed to encapsulate CBD, in which the drug is noncovalently attached to the nanosystem structure [14]. In contrast to these nanosystems, the incorporation of CBD into a nanosystem device *via* a covalent bond could provide a highly interesting and novel bioactive material. Remarkably, to the best of our knowledge, no precedents are found in the literature [15–17].

Covalent attachment of drugs to polymers has been mostly studied towards the preparation of polymer-drug conjugates (PDCs), which are

* Corresponding author at: Dept. of Organic Chemistry, Faculty of Sciences, University of Málaga, 29071, Málaga, Spain.
E-mail address: jmromero@uma.es (J. Manuel López-Romero).

https://doi.org/10.1016/j.eurpolymj.2024.113328
Received 8 March 2024; Received in revised form 16 July 2024; Accepted 19 July 2024
Available online 6 August 2024

drug delivery systems where one or more drug(s) are covalently attached to the functional groups of the polymer directly or through a spacer. PDCs have been devoted to the tailored conjugation of targeting ligands (e.g., enzymes, antibodies, peptides) to drug carrier systems, and various polymer-drug conjugates based, for example, on polyethylene glycol (PEG), *poly-N*-(2-hydroxypropyl)methacrylamide (PHPMA) [18], or superparamagnetic iron oxide nanoparticles (SPION) have been explored [16]. Among the drugs, camptothecin and doxorubicin have been two of the most studied in PDC systems [16]. In all these cases free active drug can be released directly by degradation of the spacer or by the cleavage of the drug-polymer linkage, consisting of a thermo- or pH-degradable bond, an amide linkage, a redox-cleavable bond, or an enzymatically cleavable bond.

Less studied is the use of polymers as pharmacologically active agents, which are known as polymeric drugs (PDs). PDs have found therapeutic uses as sequestrants, antimicrobials, antivirals, anticancer and anti-inflammatory agents [19]. Benefits of PDs are associated with their macromolecular character and their ability to promote biologically relevant multivalency processes. Syntheses of PDs are usually directed towards the preparation of structurally modified polymers, but also to the obtention of co-polymers holding an active drug intercalated with a monomer. For example, Li et al. studied the effect of biodegradability on CXCR4 antagonism, transfection efficacy and antimetastatic activity of polymeric plerixafor [20].

Over the years, our group has been working in the development of systems and methodologies for the delivery of drugs, making special emphasis on core@shell and hollow nanoparticles incorporating drugs against colon and lung cancers [21–23]. Since CBD has not been used to date as a monomer towards the preparation of co-polymers with applications as polymeric drugs, we decided to explore the synthesis and activity of CBD co-polymeric systems. We chose 4-vinyl pyridine as co-monomer because of the biocompatibility and water solubility properties. In this work, we wish to report our results concerning the synthesis and characterization of *poly*-4VP-co-CBD solid nanoparticles, and the analysis of the *in vitro* cytotoxicity against human and mice tumoral cell lines.

2. Experimental

2.1. Synthetic methods and materials

2.1.1. Materials

4-Vinylpyridine (4VP, 95 %) and 2,2′-azobis(isobutyronitrile) (AIBN, 98 %) were purchased from Aldrich. *N,N′*-Methylenebisacrylamide (BIS, 98 %) was supplied by Fluka. 2,2′-Azobis(2-methylpropionamidene) dihydrochloride (V50, 98 %) was purchased from Acros Organics. All reactants were used without further purification. *Cannabis sativa* dried plant having low content in tetrahydrocannabinol (THC) and high content in cannabidiol (CBD) was provided by Bhalutek Sens S.L. (Málaga, Spain). The inflorescences (clusters of flowers) were used for extraction and isolation of CBD, according to the procedure detailed in Supporting Information (SI, SI.1) [24]. CBD was purified by column chromatography to reach > 97 % (HPLC, SI.2). *Poly*-4VP was synthesized according to reference [25]. Water was purified using a Milli-Q system (Millipore).

2.1.2. Methods

For TEM imaging, a JEOL JEM1400 TEM microscope operated at 100 KV was employed. Colloidal solutions for TEM analyses were prepared by adding water (2 mL) to the lyophilized sample of solid@*poly*-4VP-co-CBD (2 mg). An aliquot of 10 μL of each colloidal solution was dropped on 100 mesh copper TEM grids and left to dry. EDX mappings were conducted by using a FEI Talos F200X (FEI, USA) equipped with an EDX detector by Bruker Nano GmbH, Germany.

For chemical composition analyses, NMR were recorded in a Bruker Advanced III 500 spectrometer. The ^{1}H spectra were recorded at 500 MHz. Chemical shifts are given relative to residual DMSO-H_6 ($\delta_H = 2.50$ ppm) in DMSO-d_6.

The Raman spectra were acquired using a near-infrared (NIR) diode laser at 785 nm Invia Qontor Raman Confocal (RENISHAW). Grating was 1200 L/mm, with slit opening at 65 μm, spectral resolution ± 1 cm and a camara CCD Renishaw Centrus as detection system.

For molecular mass distributions a MALDI-TOF/TOF UltrafleXtreme (Bruker Daltonics) was used. 2,5-Dihydroxybenzoic acid (DHB) or α-cyano-4-hydroxy-cynamic acid (CHCA) were used as matrixes. All spectra were obtained in the positive ion mode using an accelerating voltage of 8 kV for the first source and 15 kV for the second source and a laser intensity of ~ 10 % greater than threshold. Samples used for the MALDI analyses were prepared as follows: 10 mL of polymer solution (3 – 4 mg/mL in $CHCl_3$) were mixed with 30 mL of DHB or CHCA solution (0.1 M in $CHCl_3$/THF 90/10 v/v). This solution was added to 1 mL of a 0.01 M solution of CF_3COONa salt as cationizating agent, in THF as solvent. Then 1 mL of each analyte/matrix/salt mixture was spotted on the MALDI sample holder and slowly dried to allow analyte/matrix co-crystallization.

2.1.3. Synthesis of solid@poly-4VP-co-CBD

Under an Ar atmosphere, in a 100 mL round bottom flask, a mixture of EtOH (96 %, 10 mL), BIS (31.2 mg, 0.2 mmol), CBD (31.45 mg, 0.1 mmol), 4VP (430 μL, 0.988 g/mL, 4.0 mmol) and radical initiator (V50 or AIBN, 200 μL of a solution of 37 or 22 mg, respectively, in 5 mL of water, 27 mM) was refluxed (70 °C bath) for 2 h. Additional V50 or AIBN (200 μL) was added at 30, 60 and 90 min. Reaction was followed by TLC (hexanes:EtOAc, 10:1). After the reaction was completed (2 h), the mixture of reaction was concentrated to dryness under vacuum to obtain a yellowish solid. The residue was dissolved in a mixture of water: methanol (25:1 mL) and extracted with CH_2Cl_2 (3 x 25 mL) to remove any excess of CBD, BIS, 4VP and V50 or AIBN. The milky aqueous phase was centrifuged at 7000 rpm for 25 min. Solid residue was resuspended in water and centrifuged one more time. Final residue was lyophilized to obtain solid@*poly*-4VP-co-CBD as a light orange solid (58.9 mg).

2.1.4. Lyophilization

Lyophilized samples were prepared Labogene ScanVac CoolSafe apparatus. Residual solids resulting from polymerization were frozen by fast immersion in liquid nitrogen for 5 min and then transferred directly to the freeze drier using a reduced pressure ($<1 \times 10^{-3}$ bar) for 24 h.

2.1.5. Solubility

We analyzed the solubility in water of the solid@*poly*-4VP-co-CBD sample. Known amounts of the solid nanosystem in the range of 2 to 10 mg were added to the water (5 mL) at 21 °C (samples of 2.3, 5.5, 6.7, 7.8, 8.9 and 10.0 mg in 5 mL of water). Samples were sonicated during 10 min to disaggregate the solid, and then, they were stirred during 7 days at 21 °C. After this period, the samples were filtered off through a 0.8 μm filter (MCE Millex®) to remove any residual solid.

2.2. Antitumoral assays

2.2.1. Cell culture

In this study, A549 human lung adenocarcinoma epithelial cell line from the Instrumentation Service Center of the University of Granada (Spain) was used as a model of non-small cell lung cancer (NSCLC). Cells were growth in Dulbecco's Modified Eagle's Medium (DMEM)-high glucose (Sigma-Aldrich) supplemented with 10 % Fetal bovine serum (FBS) and 1 % penicillin–streptomycin, with air containing 5 % CO_2 and 37 °C.

2.2.2. Cytotoxicity assay

A549 cells were grown with completed DMEM in 48-well plates at a density of 5 x 103 cells per well. 24 h later, cell cultures were exposed to increasing concentrations of the drugs (CBD or solid@*poly*-4VP-co-CBD)

up to a maximum value of 50 μM for 72 h with air containing 5 % CO_2 and 37 °C. Quantification of cytotoxicity was performed with a colorimetric assay with MTT. Cells were incubated for 3 h with MTT solution (5 mg MTT / 1 mL PBS) at 10 % well volume until formazan crystals were formed. These crystals were dissolved with a DMSO:Sorensen solution (8:1) for the measurement of the optical density (OD) at 570 and 630 nm. The relative inhibition (%) was calculated with the formula:

$$Relativeinhibition(\%) = 100 - \left(\frac{(ODsample570 - ODsample630) - blank}{(ODnegative570 - ODnegative630) - blank} * 100 \right) \quad (1)$$

2.2.3. Wound-healing assay

A wound healing assay was performed to quantify the modulation capacity of the drugs on cell migration. Cells were seeded in 1 mL of completed DMEM at a density of 3 x 105 in 12 well-plates and incubated for 24 h to ensure adherence and 100 % confluence. After 24 h, the well diameter was profiled with a 100 μL pipette tip to lift the cells from the well, subsequently washing the well with PBS to remove detached cells. Once the wells have been washed, the cells were incubated in FBS-free DMEM for 72 h at 5 % CO_2 and 37 °C in the presence of the drugs at concentrations of IC5 and IC10, obtaining images at different times (0, 24, 48 and 72 h) with an inverted light microscope Olympus CKX41. These images were analyzed with the Wound Healing Tool extension of ImageJ software to obtain the cell-free well area.

2.2.4. Clonogenic assay

Cells were incubated in 6-well plates at a density of 1 x 10^5 cells in 1.5 mL of complete DMEM per well. After 24 h, drugs (CBD or solid@*poly*-4VP-co-CBD) were added at IC50 concentrations for both drugs and IC70 for solid@*poly*-4VP-co-CBD and incubated for 72 h at 5 % CO_2 and 37 °C. The surviving pre-treated cells were detached with a trypsin: PBS-EDTA solution (1:2) at 37 °C. Once the cells have been detached, they were incubated in 12-well plates at a cell density of 2 x 10^2 / well in 1 mL of DMEM and incubated for approximately 7 days at 5 % CO_2 and 37 °C. Then, the cells were fixed for 20 min at 4 °C with 10 % trichloroacetic acid (TCA) and subsequently stained with 0.08 % sulforhodamine B solution (Sigma-Aldrich) diluted in 1 % glacial acetic acid (PanReac AppliChem). The results have been represented as number of colonies observed and as percentage of colony formation following the formula (2):

$$Colonyformation(\%) = \frac{Numberofcoloniesformed}{Numberofcellsseededinawell} \quad (2)$$

2.3. ^1H NMR data

$_{\delta H}$ **CBD** (DMSO-d_6) ppm: 8.65 (brs, 2H, 2 x OH), 6.02 (s, 2H, H-3′, H-6′), 5.09 (s, 1H, H-2), 4.51 (s, 1H, =CHH), 4.42 (s, 1H, =CHH), 3.83 (m, 1H, H-1), 3.03 (m, 1H, H-6), 2.30 (m, 2H), 2.08 (m, 1H), 1.91 (m, 1H), 1.65–1.52 (m, 2H), 1.52 and 1.53 (2 x s, 2 x 3H, CH_3-7 and CH_3-9), 1.48 (m, 2H) 1.27 (m, 4H), 0.87 (t, 3H, J = 7.0 Hz, CH_3-5′′).

$_{\delta H}$ **BIS** (DMSO-d_6) ppm: 8.75 (sa, 2 x NH, 2H), 6.26 (dd, J = 17.1, 10.1 Hz, 2H, H-2), 6.14 (dd, J = 17.1, 2.3 Hz, 2H, H-3), 5.62 (dd, J = 10.1, 2.2 Hz, 2H, H-4), 4.55 (t, J = 6.0 Hz, 2H, CH_2).

$_{\delta H}$ **4VP** (DMSO-d_6) ppm: 8.68–8.30 (m, 2H, H-2), 7.47–7.28 (m, 2H, H-3), 6.68 (dd, J = 17.7, 10.9 Hz, 1H, H-5), 6.06 (d, J = 17.6 Hz, 1H, H-7), 5.46 (d, J = 10.9 Hz, 1H, H-6).

$_{\delta H}$ **solid@*poly*-4VP-co-CBD** (DMSO-d_6) ppm: 8.27 (brs, 104H, PyH, OH, NH), 6.70 (brs, 104H, PyH, ArH), 5.17 (brs, 1H, C = CH), 4.43 (brs, 3H, NCH_2N), 3.4–0.9 (m, aliphatic protons), 0.87 (t, 3H, terminal CH_3).

3. Results

3.1. Synthesis of CBD co-polymeric nanoparticles (solid@poly-4VP-co-CBD)

poly-4VP is a pH-responsive and biocompatible microgel, which has been extensively used as drug delivery system, and as coating shell for nanosized cores such as metal or magnetic nanoparticles, providing numerous advantages, for example, in sensing and catalysis applications [23,25,26]. In aqueous media, *poly*-4VP is normally prepared by free radical polymerization of 4VP monomers in presence of a cross-linker (*N,N'*-methylenebisacrylamide, divinylbenzene, or ethylene glycol dimethacrylate) and using 2,2′-azobis(2-methylpropionamidene) or ammonium or potassium persulfate as radical initiator agents [27,28]. In case of co-polymeric systems, the polymerization of 4VP has been carried out over colloidal particles of gold, SiO_2, or polycaprolactone, all of them acting as a core for the polymer shell. For example, co-polymeric nanoparticles of 4VP and *poly*(methacrylic acid) (PMA) have been prepared. In this case, hollow@*poly*-4VP-co-PMA systems were obtained by using SiO_2 nanoparticles as polymerization core [29]. A *poly*-styrene core has also been used for the preparation of hollow nanoparticles [30].

Following the reported procedures, we prepared the 4VP and CBD co-polymer (solid@*poly*-4VP-co-CBD) by radical polymerization using 2,2′-azobis(2-methylpropionamidene)dihydrochloride (V50) as reaction initiator and *N,N'*-dimethylenebisacrylamide (BIS) as cross-linker. Reaction was carried out by refluxing during 2 h the monomer 4VP and co-monomer CBD in presence of BIS and V50 in ethanol (Scheme 1). BIS was used in 5 mol% with respect to 4VP, while CBD in 2.5 mol% with respect to 4VP. Water was also tested as solvent, however, there was not a complete dissolution of reagents at 70 °C and, even when polymerization was observed, only amorphous polymer was obtained by precipitation. When AIBN was used as radical initiator, similar results to the use of V50 were obtained. Lyophilized solid@*poly*-4VP-co-CBD nanoparticles were characterized by Raman, TEM and NMR.

Morphology of the co-polymeric NPs was studied by TEM. Fig. 1 shows two representative TEM images of the isolated solid@*poly*-4VP-co-CBD systems and the corresponding histogram. Initial analysis of selected images (ImageJ software) showed a high degree of

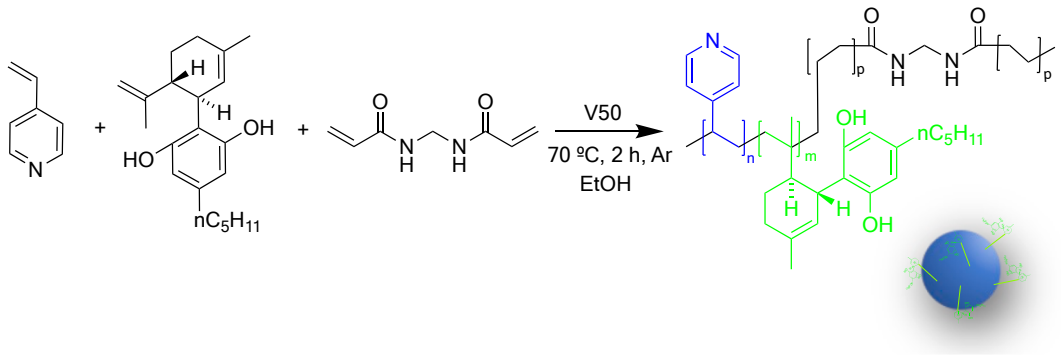

Scheme 1. Synthesis of solid@*poly*-4VP-co-CBD.

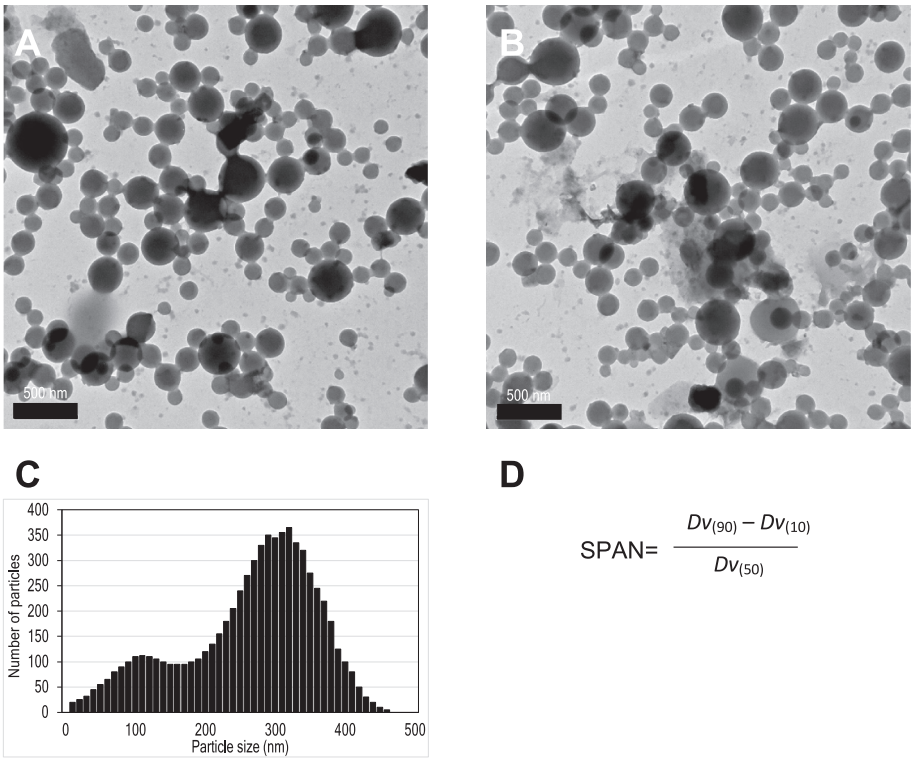

Fig. 1. A and B) TEM images of solid@*poly*-4VP-co-CBD; C) sizes histogram, which shows mean values obtained from the analysis of two representative images; and D) SPAN formula, where $Dv_{(90)}$, $Dv_{(50)}$ and $Dv_{(10)}$ are the diameters below which 90 %, 50 % and 10 %, respectively, of the NPs is contained.

polydispersity for the prepared samples. However, a deeper study of the sizes of the NPs, showed a good fit into a binomial distribution, where two main average values for the external diameters were found, 275 ± 5 nm for the bigger NPs and 85 ± 2 nm for smaller ones, being in a ratio of about 1.7 big/small, and with SPAN polydispersity indices of 0.55 and 0.75 respectively (see formula in Fig. 1).

Qualitative chemical composition of the nanoparticles has been studied by comparison among the Raman spectra of neat *poly*-4VP and CBD with the corresponding co-polymeric system (Fig. 2). Raman spectroscopy has been recently reported as a rapid and worthwhile technique for the *in situ* detection of cannabinoids in *Cannabis sativa* L [31]. CBD presents two intense and characteristics vibrational absorption bands at 1663 and 1440 cm^{-1}, assigned to the bending vibration of the aliphatic chain and $_{\delta}(CH_2)$ and $_{\delta}(CH_3)$ also of the aliphatic chain, respectively. In the high wave number region, the symmetric and asymmetric stretching vibrations of methylene groups $\sigma(CH_2)$ are detected at 2870 and 2970 cm^{-1}. All these vibrational modes are observed in the Raman spectra of the co-polymeric systems incorporating CBD. Fig. 2 shows the Raman spectra for neat *poly*-4VP (Fig. 2A) [25], solid@*poly*-4VP-co-CBD (Fig. 2B), and neat CBD (Fig. 2C), recorded over lyophilized samples. It can be seen the presence of the characteristics bands of CBD, marked with red arrows, and these of *poly*-4VP (green arrows) in the Raman spectra of solid@*poly*-4VP-co-CBD (Fig. 2B). It is important to note that characteristics bands of CBD at 1440, 1663, 2870 and 2970 cm^{-1} are now shifted to 1450, 1700, 2850 and 3110 cm^{-1}, thus confirming the covalent bond formation during polymerization, and the incorporation of the drug to the *poly*-4VP matrix. This effect also can be observed in the *poly*-4VP bands, mainly these intense bands at 620, 750 and 1070 cm^{-1} (Fig. 2A, green arrows), the last assigned to CH in plane bending [30], now appearing in the co-polymer at about 720 cm^{-1}, as a new band, and 1125 cm^{-1} (Fig. 2B, green arrows).

The possibility of using this technique for the study of nanoparticle structure and composition should be pointed out since only few publications have been reported to date.

Chemical composition of solid@*poly*-4VP-co-CBD and *poly*-4VP was also studied by High-Angle Annular Dark-Field TEM (HAADF-TEM) and EDX elemental mapping analysis (Fig. 3). Nanoparticles structure can be clearly distinguished for solid@*poly*-4VP-co-CBD (Fig. 3A-D) and *poly*-4VP (Fig. 3E-H) systems.

The EDX spectrum extracted from the TEM images of Fig. 3C (solid@*poly*-4VP-co-CBD) showed a percentage of C, N and O of 92.3, 4.2 and 3.5 %, respectively, while spectrum extracted form Fig. 3G (*poly*-4VP) showed a percentage of C, N and O of 92.5, 4.9 and 2.6 %, respectively. As expected, solid@*poly*-4VP-co-CBD samples showed a minor N percentage, about 14 % less, due to the presence of CBD in the polymer structure. These results are in concordance with the ratio of monomer, co-monomer and crosslinker used during the synthesis (see Experimental for details).

^{1}H NMR was used as a technique to confirm the chemical composition of solid@*poly*-4VP-co-CBD, providing direct evidence of the successful co-polymerization. Moreover, integrals have been used to calculate the 4VP:CBD ratio in the co-polymer. Fig. 4 shows the ^{1}H NMR spectra recorded in DMSO-d_6 of samples of co-polymer, neat CBD, BIS and 4VP. The spectrum of the co-polymer solid@*poly*-4VP-co-CBD shows its characteristic peaks, including a triplet at 0.87 ppm, assigned to the terminal methyl group of the five carbons aliphatic chain (H-5′′ protons) and a signal at about 5.17 ppm, corresponding to the cyclic vinyl proton (H-2, integral 1.0), both of the CBD moiety, together with three broad signals centered at 8.27, 6.70 and 1.53 ppm, corresponding to the heterocyclic moiety, and methylene groups, presents in the BIS crosslinked *poly*-4VP structure. As it can be seen, in the ^{1}H NMR of solid@*poly*-4VP-co-CBD, the doublet signals at 4.51 and 4.42 ppm corresponding to the exocyclic double bond of CBD, are not observed, meaning a successful covalent linkage through this bond during polymerization. A more hindered intracyclic double bond can explain the observed regioselectivity. From the comparison of the integrals of co-polymer H-2 signal, which clearly appears without overlapping signals (1H, 5.17 ppm) and the signals of pyridine protons (2H, 6.70 ppm,

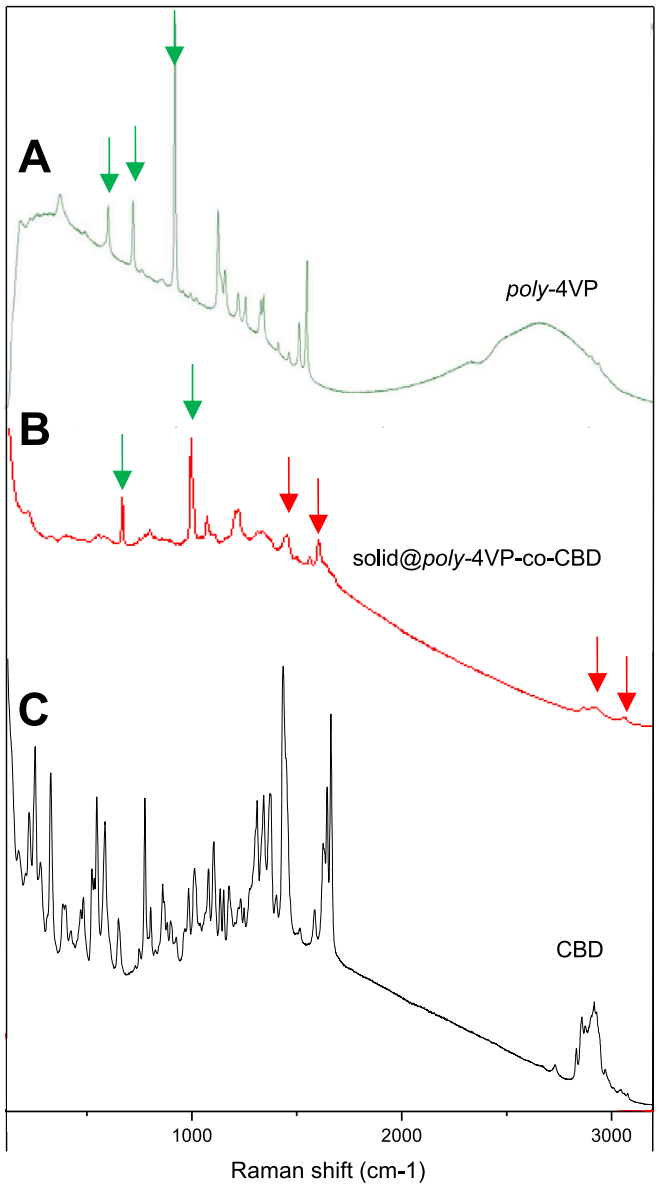

Fig. 2. Raman spectra (785 nm laser line) of A) *poly*-4VP; B) solid@*poly*-4VP-co-CBD co-polymer, and C) neat CBD.

integral 104) the ratio CBD:4VP was estimated in 1:52, which is concordance with the quantities used during polymerization.

In order to obtain detailed information about the chemical structure, co-polymer mass was analyzed by MALDI-TOF/TOF spectrometry, using DHB or CHCA as matrixes, obtaining similar results in both cases. Fig. 5 includes the spectra recorded using DHB as matrix. The species observed are consistent with the monomer ratios used for synthesis. Fig. 5A shows the MALDI spectrum of *poly*-4VP, where it can be seen and maximum molecular mass of 767 Da, and the recurrent loss of 105 Da, consistent with the molecular mass of 4VP. Fig. 5B shows the spectrum for solid@*poly*-4VP-co-CBD, with a mass of 871 Da and the loss of fragment 315 Da associated to CBD.

3.2. Solubility

CBD has very low water solubility (12.6 mg/L) and high lipophilicity, with a value 6.3 for the log P, being log P the logarithm of a drug's partition coefficient between *n*-octanol and water. Since solubility in water and hydrophilic solvents is necessary for biological applications of active compounds, many efforts have been carried out to develop CBD formulations with an improved solubility, including polymeric micelles and nanoparticles (PLGA and zein/whey protein), hybrid nanoparticles jelled in cross-linked chitosan, and lipid formulations, such as nanostructured lipid carriers, vesicles, or nano- and microemulsions [32].

We carried out a preliminary study on the solubility of the co-polymeric systems by conducting an equilibrium solubility test. Samples of the nanosystem, in the range of 2 to 10 mg, were added to 5 mL of water, and then stirred during 7 days at 21 °C to reach a solubility equilibrium. We have found that solid@*poly*-4VP-co-CBD forms stable emulsions in quantities up to 7.8 mg in 5 mL of water, while at concentrations of 8.9 mg/mL and higher it was always observed a precipitated solid (see images in Supporting Information, Figure SI.3), which can be removed by filtration. Moreover, a clear solution was obtained when concentrations are less or equal to 2.3 mg in 5 mL of water. It means that the solubility in water for this polymeric drug is about 37 times higher than that for the free CBD. The improved water solubility can be explained by the interaction of pyridine nitrogen atom with water hydrogens, allowing the solubilization of hydrophobic drugs. Moreover, it was observed that the nanoemulsions were stable during a period of four weeks of storage at room temperature (21 °C) and protected from light.

3.3. Solid@poly-4VP-co-CBD maintains CBD cytotoxic properties against A549

Cytotoxic tendency at increasing concentrations of the different drugs was represented in Fig. 6. The cytotoxic capacity of CBD was greater in the free form, although the IC50 of CBD (Fig. 6A) and solid@*poly*-4VP-co-CBD (Fig. 6B) were very close, with values of 15.99 ± 0.41 and 16.99 ± 8.09, respectively. Moreover, the toxicity of the solid@*poly*-4VP-co-CBD systems remain reduced despite slight growth at higher concentrations, confirming the safety of the nanoformulation (Fig. 6C). Since the solid@*poly*-4VP does not exert a toxic effect, it can be stated that the observed cell death is mostly due to the ability of CBD to activate apoptosis, even being covalently attached to the polymer matrix. In fact, it has been demonstrated that CBD is able to increase mitochondrial Ca^{2+} because of interaction with mitochondrial ion channels, allowing the release of cytochrome *C* into the cytoplasm and triggering caspase-9-mediated apoptosis [9]. This drug can also trigger an apoptotic response via direct activation of cytoplasmatic caspase 8 [9]. In A549 cells, an activation of the PPAR-γ apoptotic pathway has also been observed as a consequence of cyclooxygenase 2 (COX2) activation [33]. In addition to the apoptotic response, cells experience increased oxidative stress by interacting with membrane proteins NOX4 and p22phox and by inhibiting some antioxidant enzymes such as superoxide dismutase or catalase [9]. Because the solvent of the drugs was DMSO, its effect alone was tested, being the highest dose tested in drugs a maximum DMSO percentage of 1.32 %, present in the 50 μM solid@*poly*-4VP-co-CBD treatment (Fig. 6). In all three cases, a certain toxicity of DMSO can be observed, although was more important in the case of solid@*poly*-4VP-co-CBD because it was the solution with the lowest concentration. Despite this, the toxicity of DMSO at concentrations close to the IC50 of solid@*poly*-4VP-co-CBD was low, so the toxicity observed in the Fig. 6A is mostly due to the activity of the drug.

3.4. Solid@poly-4VP-co-CBD is not able to inhibit cell migration

As shown in Fig. 7, a 58 % reduction was observed in cell migration capacity after free CBD exposure at a IC5 concentration. This effect was previously demonstrated *in vitro* and *in vivo* using with A549 cells [34,35]. In addition, the migration did not significantly modify between the doses of IC5 and IC10. However, this effect on migration was not observable when the cells were exposed to co-polymeric CBD. Interestingly, the effect of CBD depends on its interaction with TRPV1, CB1 and

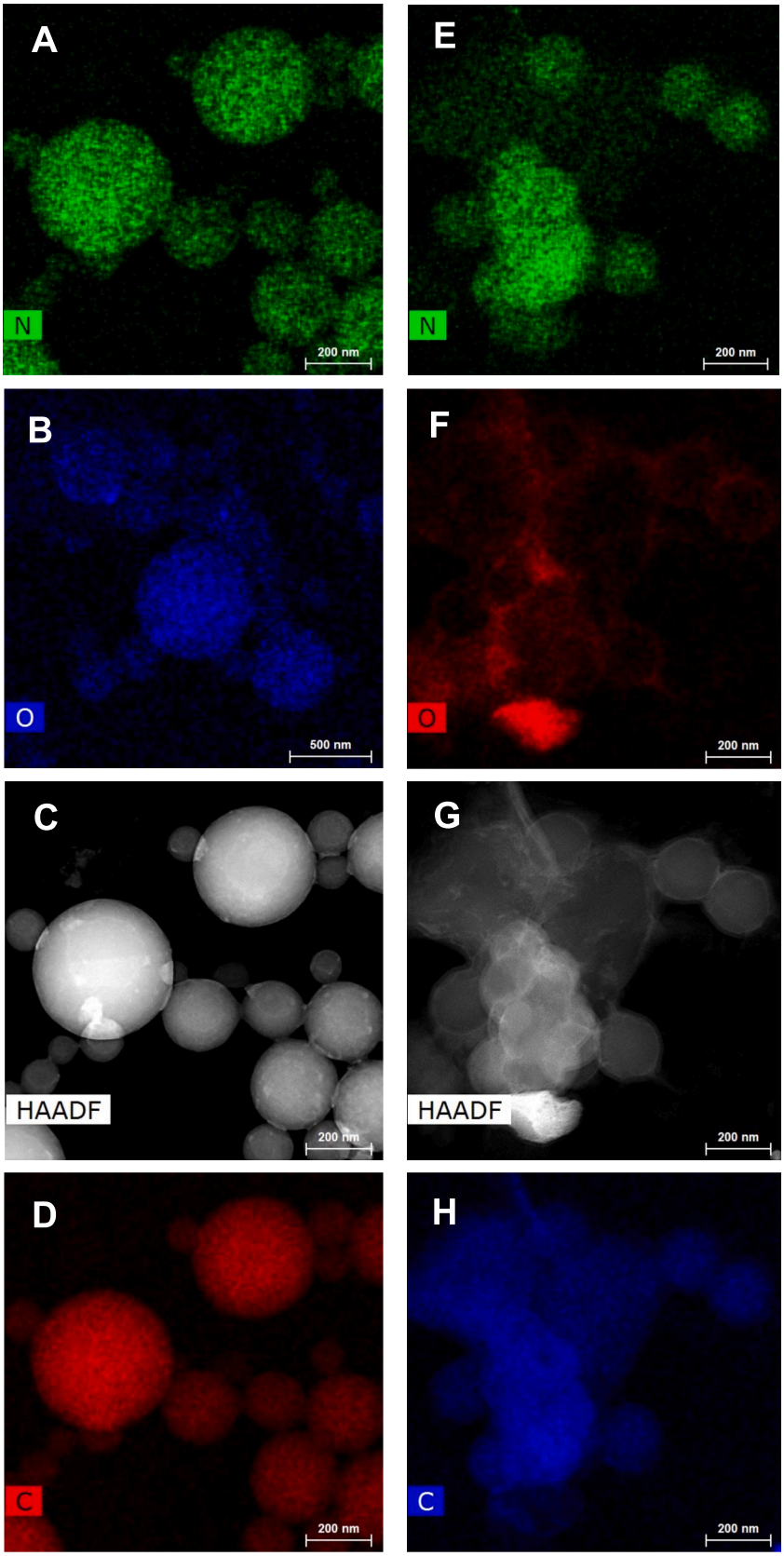

Fig. 3. HAADF-TEM mapping images of solid@*poly*-4VP-co-CBD system (A-D), and for neat *poly*-4VP (E-H).

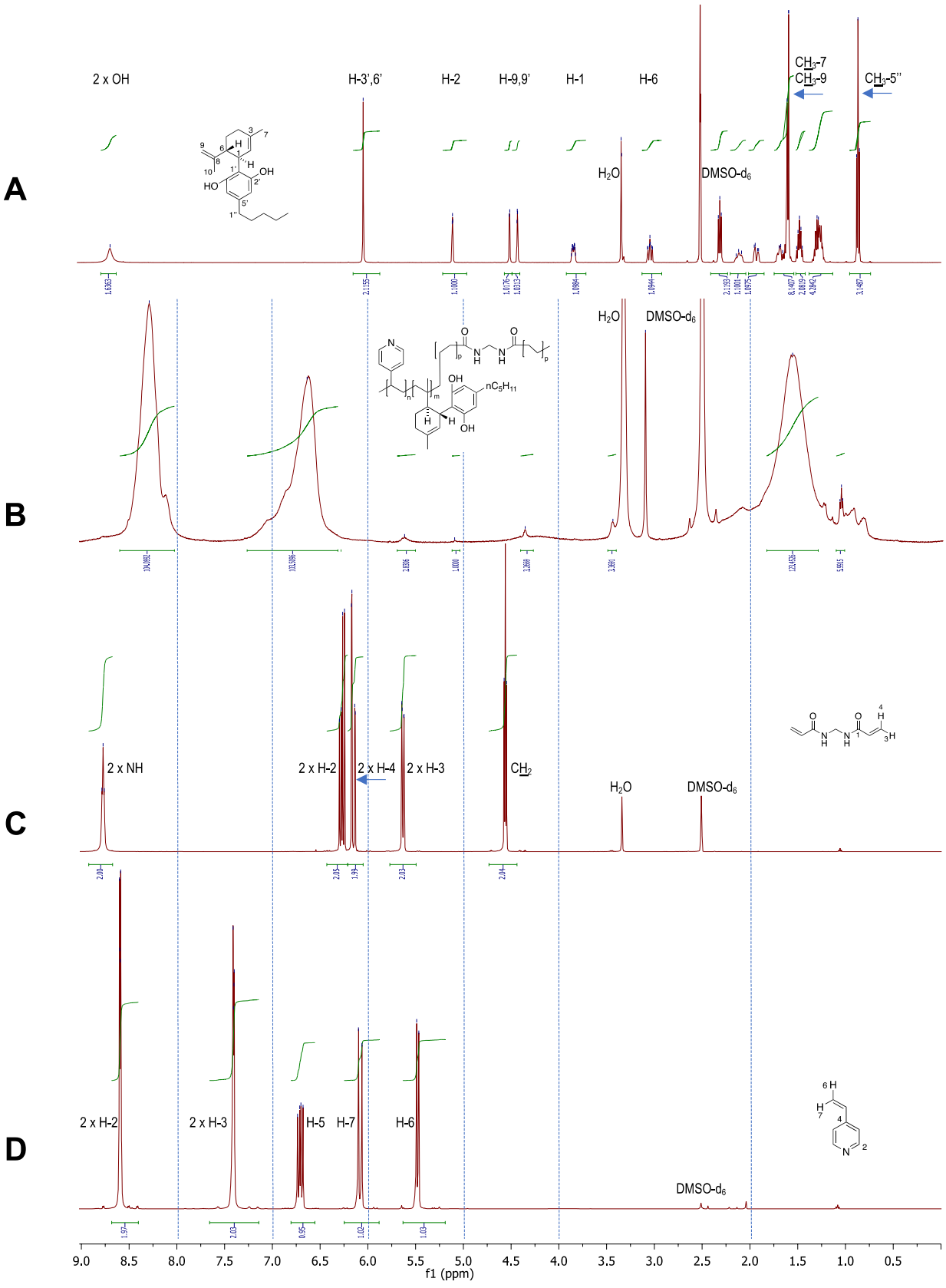

Fig. 4. ^{1}H NMR of A) neat CBD (DMSO-d_6), B) solid@*poly*-4VP-co-CBD (DMSO-d_6), C) BIS (DMSO-d_6) and D) 4VP (DMSO-d_6).

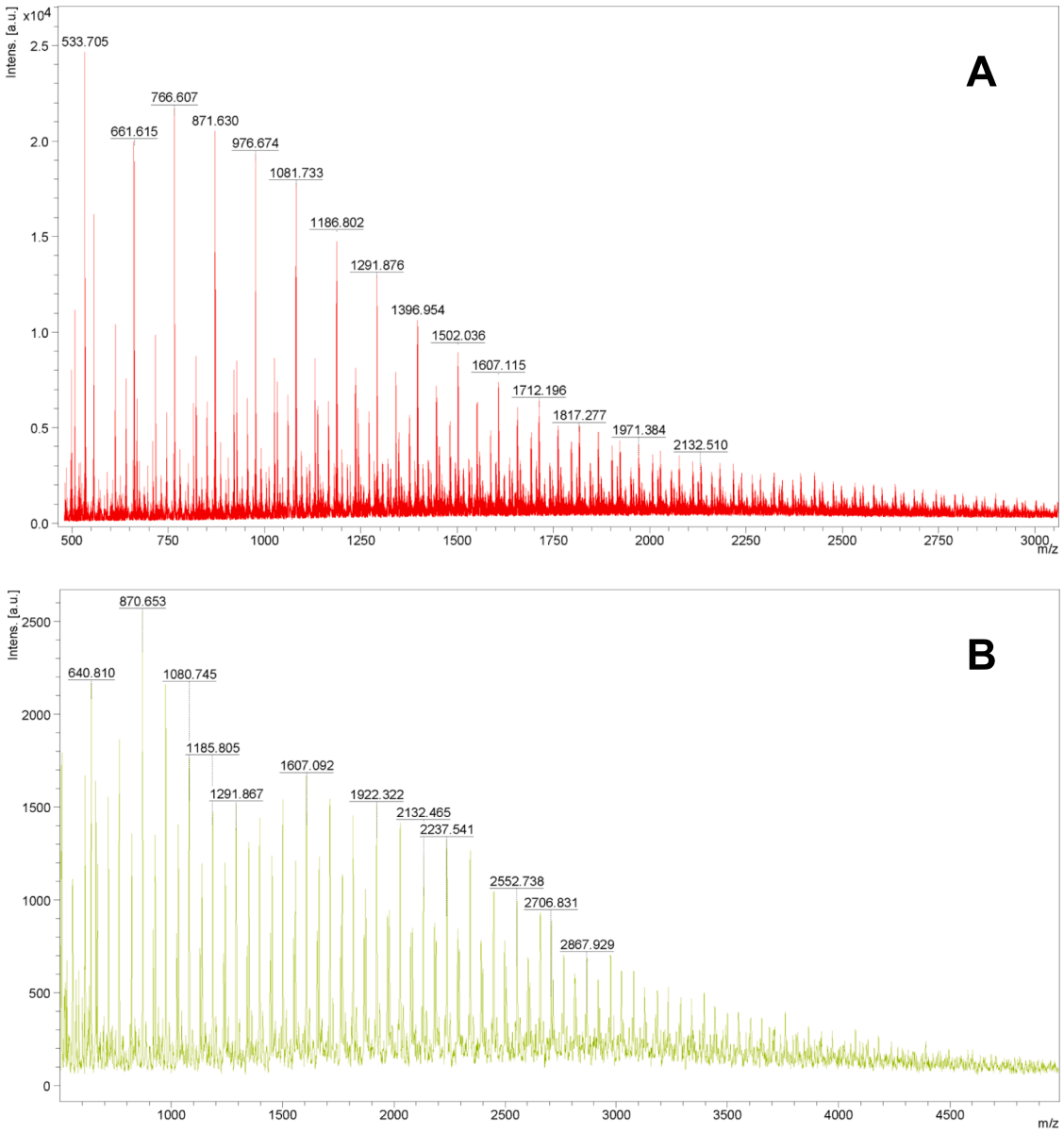

Fig. 5. MALDI-TOF/TOF spectra of A) neat *poly*-4VP, B) solid@*poly*-4VP-co-CBD (DHB matrix).

CB2 A549 membrane receptors, which increase the levels of ICAM-1 (intercellular adhesion molecule 1) by activating signaling pathways. In fact, this increase in ICAM-1 levels allows an increase in the levels of TIMP-1 (tissue inhibitor of MMPs), a protein involved in the reduction of invasiveness [9,36,37]. Then, the exclusive localization of A549 receptors in cell membrane could justify the inability of CBD to exert a negative effect on migration when it is covalently bonded to *poly*-4VP matrix.

3.5. Solid@poly-4VP-co-CBD enables CBD to act as an inhibitor of colony formation

As shown in Fig. 8A, colony formation of surviving pre-treated A549 cells after 72 h exposure to CBD is totally inhibited at an IC50 concentration. On the other hand, treatment with solid@*poly*-4VP-co-CBD causes an inhibition of colony formation but does not reach the values of the free CBD. This result may be related to the inhibition that CBD exerts in EGFR (epidermal growth factor receptor) and GPR55 (G protein-coupled receptor 55) receptors. This fact was clearly observed in the treatment of breast cancer with this drug [38,39]. This colony formation inhibition effect has been demonstrated in some lung cancer cell lines such as A549, H640 and H1792, as well as in other types of cancer such as bone, prostate, or breast cancer [35]. Thus, the difficulty of the polymeric drug to interact with membrane receptors may account for this difference in colony formation, even when many of the CBD moieties can be considered to be on the surface of the nanosystem. Even so, CBD also presents the capacity to act in the cytoplasm increasing the production of MTROC1 inhibitory factors (such as PPAR-γ and p53) or influencing the activity of some molecules involved in proliferation [9,33], which would explain the capacity of solid@*poly*-4VP-co-CBD to exert this activity. Finally, the inhibition in colony-forming ability was dose dependent, since IC70 concentrations of solid@*poly*-4VP-co-CBD inhibited 3.5 times more than IC50 concentrations of solid@*poly*-4VP-co-CBD (Fig. 8B).

4. Conclusions

We have synthesized 4VP co-polymeric CBD using *N,N'*-methylenbisacrylamide as cross-linker, in which CBD is covalently incorporated to the polymeric structure (solid@*poly*-4VP-co-CBD). We

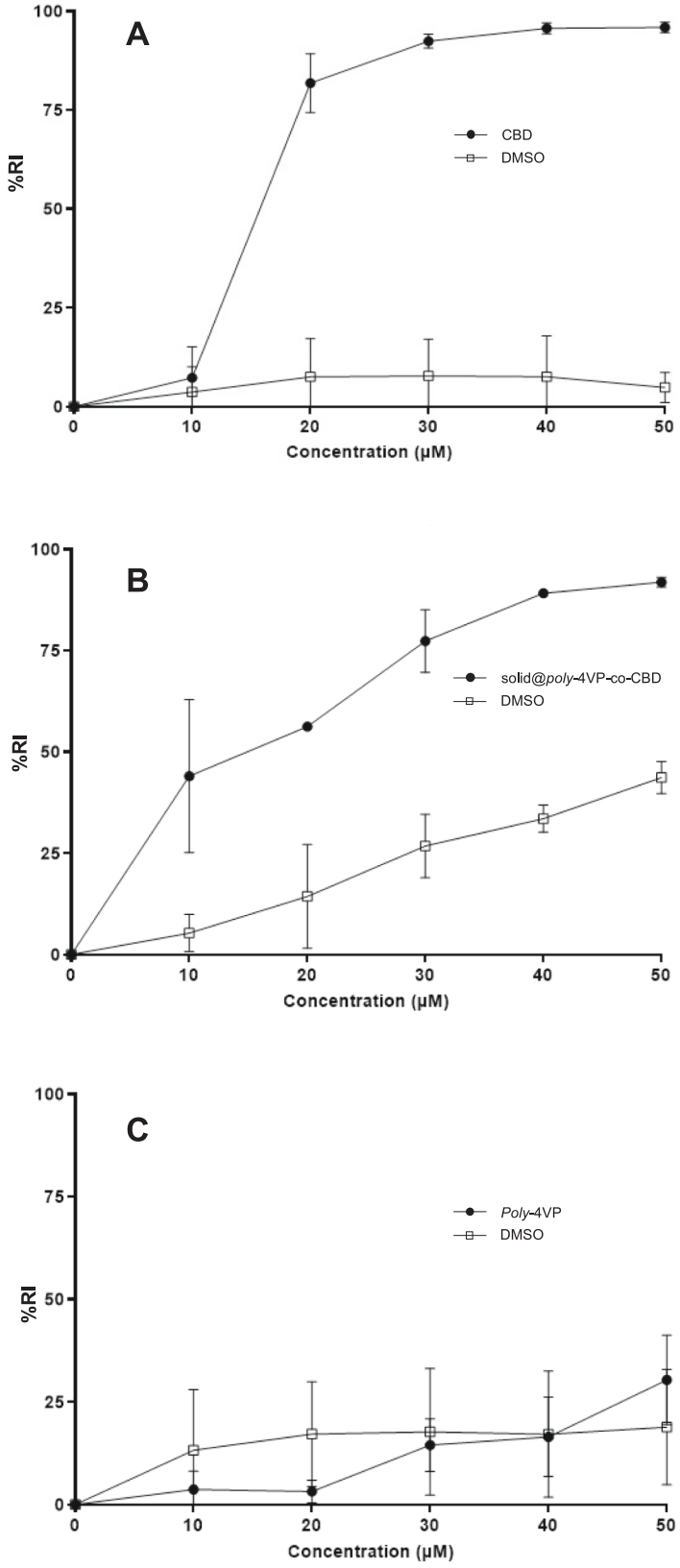

Fig. 6. Relative inhibition (% RI) at increasing concentrations of A) CBD, B) solid@*poly*-4VP-co-CBD and C) *poly*-4VP in DMSO after72 h of incubation period.

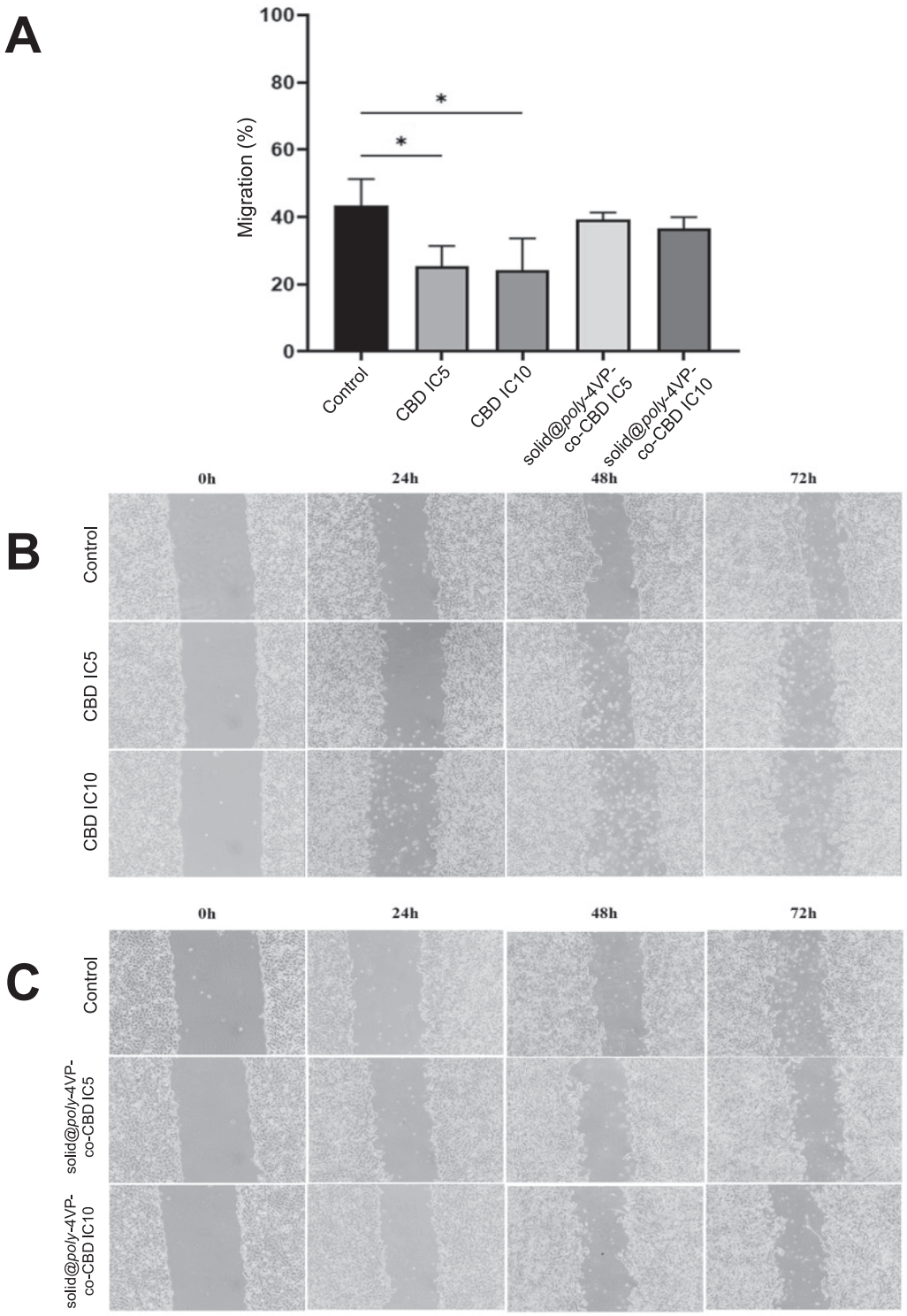

Fig. 7. A) Graphic representation of percentage of cell migration at IC5 and IC10 concentrations of CBD and solid@*poly*-4VP-co-CBD for 72 h. Evolution of cell migration with B) CBD and C) solid@*poly*-4VP-co-CBD treatments.

characterized the nanoparticle morphology by TEM, showing an average diameter of 275 nm, while the chemical composition was confirmed by ^{1}H NMR, Raman, and EDX spectroscopies, in which the ratio CBD:4VP was estimated in 1:52. Mass spectrometry also confirmed the presence of CBD in the co-polymer, which reach 871 Da. The synthesized polymeric drug improves the solubility of free CBD in about 37 times.

Activity of superficial CBD has also been tested. Antitumor effect was analyzed in human lung cell lines. The results of this biological study showed that the polymeric drug retained the cytotoxic and antiproliferative effects of CBD on a smaller scale, maintaining the cytotoxic properties against lung A549 cell lines, acting as an antiproliferative agent, but superficial CBD did not inhibit cell migration. These results demonstrated that the solid@*poly*-4VP-co-CBD system might have potential as polymeric drug to be used as an alternative to the free CBD.

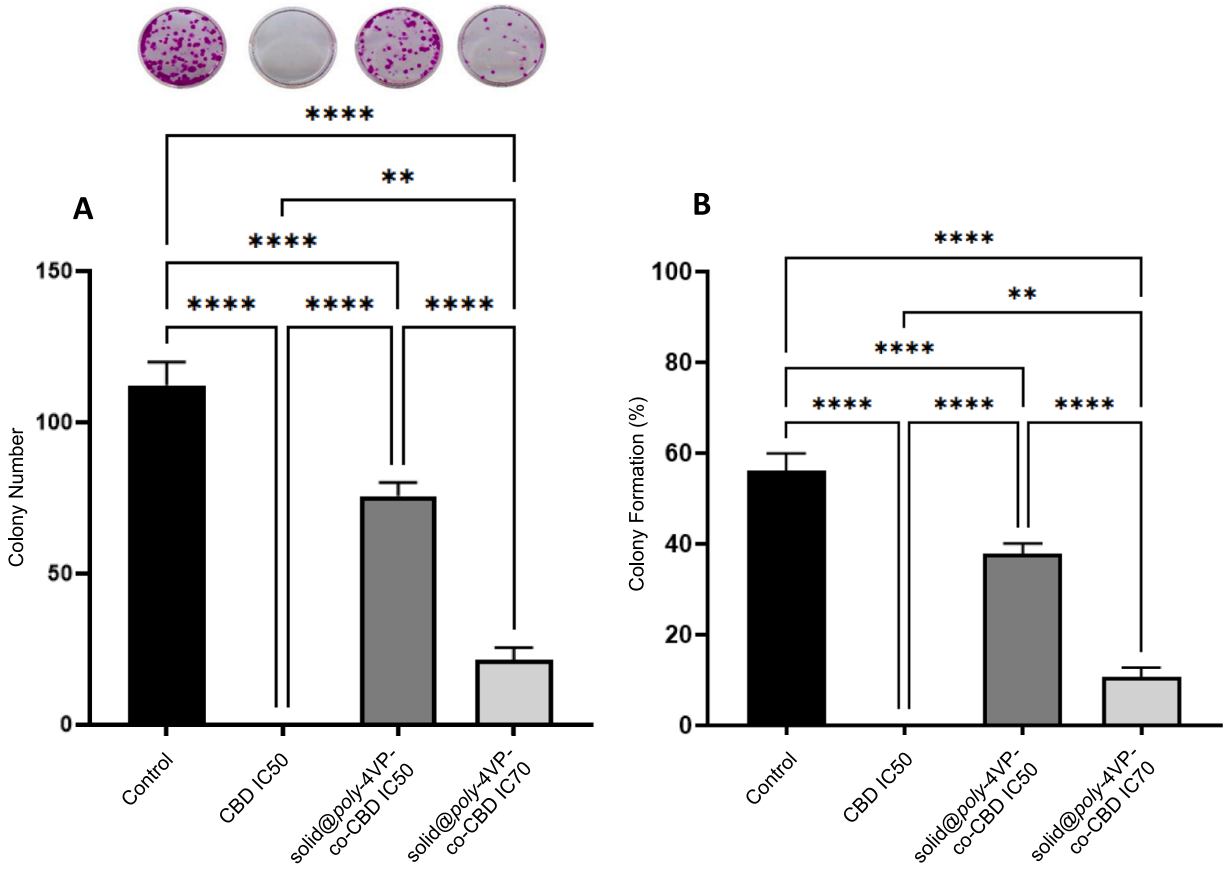

Fig. 8. Colony formation assay after 72 h incubation with CBD IC50 (16 μM) and solid@*poly*-4VP-co-CBD IC50 and IC70 (17 μM and 30 μM respectively). Graphical representation of the number of colonies (A) and percentage of colony formation (B).

Declaration of competing interest

The authors declare that they have no known competing financial interests or personal relationships that could have appeared to influence the work reported in this paper.

Data availability

Data will be made available on request.

Acknowledgments

Authors thanks Andalusian Government for financial support: FQM397 and UMA20 FEDERJA84 Projects.

Appendix A. Supplementary data

Supplementary data to this article can be found online at https://doi.org/10.1016/j.eurpolymj.2024.113328.

References

[1] A.E. Odieka, G.U. Obuzor, O.O. Oyedeji, M. Gondwe, Y.S. Hosu, A.O. Oyedeji, The medicinal natural products of Cannabis sativa Linn.: a review, Molecules 27 (5) (2022) 1689–1715, https://doi.org/10.3390/molecules27051689.
[2] R. Mechoulam, M. Peters, E. Murillo-Rodríguez, L. Hanus, Cannabidiol – recent advances, Chem. Biodivers. 4 (2007) 1678–1692, https://doi.org/10.1002/cbdv.200790147.
[3] S.C. Britch, S. Babalonis, S.L. Walsh, Cannabidiol: pharmacology and therapeutic targets, Psychopharmacol. 238 (2021) 9–28, https://doi.org/10.1007/s00213-020-05712-8.
[4] J.W. Skelley, C.M. Deas, Z. Curren, J. Ennis, Use of cannabidiol in anxiety and anxiety-related disorders, J. Am. Pharm. Assoc. 60 (2020) 253–261, https://doi.org/10.1016/j.japh.2019.11.008.
[5] R. von Wrede, C. Helmstaedter, R. Surges, Cannabidiol in the treatment of epilepsy, Clin. Drug Inv. 41 (3) (2021) 211–220, https://doi.org/10.1007/s40261-021-01003-y.
[6] S. Atalay, I. Jarocka-Karpowicz, E. Skrzydlewska, Antioxidative and anti-Inflammatory properties of cannabidiol, Antioxidants 9 (1) (2019) 21–27, https://doi.org/10.3390/antiox9010021.
[7] A. Kicman, M. Toczek, The effects of cannabidiol, a non-intoxicating compound of cannabis, on the cardiovascular system in health and disease, Int. J. Mol. Sci. 21 (18) (2020) 6740–6789, https://doi.org/10.3390/ijms21186740.
[8] S. Torres, M. Lorente, F. Rodríguez-Fornes, S. Hernández-Tiedra, M. Salazar, E. García-Taboada, G. Velasco, A combined preclinical therapy of cannabinoids and temozolomide against glioma, Mol. Cancer Ther. 10 (2011) 90–103, https://doi.org/10.1158/1535-7163.MCT-10-0688.
[9] C. Yan, Y. Li, H. Liu, D. Chen, J. Wu, Antitumor mechanism of cannabidiol hidden behind cancer hallmarks, Biochim. Biophys. Acta - Reviews on Cancer 1878 (4) (2023) 188905, https://doi.org/10.1016/j.bbcan.2023.188905.
[10] C.G. Heider, S.A. Itenberg, J. Rao, H. Ma, X. Wu, Mechanisms of cannabidiol (CBD) in cancer treatment: a review, Biology 11 (6) (2022) 817–834, https://doi.org/10.3390/biology11060817.
[11] C. Valenti, M. Billi, G.L. Pancrazi, E. Calabria, N.G. Armogida, G. Tortora, Biological effects of cannabidiol on human cancer cells: systematic review of the literature, Pharmacol. Res. 181 (2022) 106267, https://doi.org/10.1016/j.phrs.2022.106267.
[12] C. Wang, B. Cui, Y. Sun, C. Wang, M. Guo, Preparation, stability, antioxidative property and *in vitro* release of cannabidiol (CBD) in zein-whey protein composite nanoparticles, LWT 162 (2022) 113466, https://doi.org/10.1016/j.lwt.2022.113466.
[13] H. Zheng, B. Chen, J. Rao, Nutraceutical potential of industrial hemp (*Cannabis sativa* L.) extracts: physicochemical stability and bioaccessibility of cannabidiol (CBD) nanoemulsions, Food Function 13 (2023) 4502–4512, https://doi.org/10.1039/D1FO04433H.
[14] I.D.M.D. Ramalho, D.T. Pereira, G.B.L. Galvão, D.T. Freire, L. Amaral-Machado, E. D.N. Alencar, Current trends on cannabidiol delivery systems: where are we and where are we going? Expert Opinion Drug Delivery 18 (11) (2021) 1577–1587, https://doi.org/10.1080/17425247.2021.1952978.

[15] I. Theochari, A. Xenakis, V. Papadimitriou, (Eds), Nanocarriers for effective drug delivery, Smart nanocontainers: micro and nano technologies, smart nanocontainers, Elsevier, Greece, 2020, pp. 315–341, https://doi.org/10.1016/B978-0-12-816770-0.00019-8.
[16] K. Ulbrich, K. Holá, V. Šubr, A. Bakandritsos, J. Tuček, R. Zbořil, Targeted drug delivery with polymers and magnetic nanoparticles: covalent and noncovalent approaches, release control, and clinical studies, Chem. Rev. 116 (2016) 5338–5431, https://doi.org/10.1021/acs.chemrev.5b00589.
[17] I. Klojdová, T. Milota, J. Smetanová, C. Stathopoulos, Encapsulation: A strategy to deliver therapeutics and bioactive compounds? Pharmaceuticals 16 (2023) 362, https://doi.org/10.3390/ph16030362.
[18] D. Wang, S. Miller, M. Sima, P. Kopecková, J. Kopecek, Synthesis and Evaluation of Water-Soluble Polymeric Bone-Targeted Drug Delivery Systems, Bioconjugate Chem. 14 (2003) 853–859, https://doi.org/10.1021/bc034090j.
[19] J. Li, F. Yu, Y. Chen, D. Oupicky, Polymeric drugs: Advances in the development of pharmacologically active polymers, Journal of Controlled Release 219 (2015) 369–382, https://doi.org/10.1016/j.jconrel.2015.09.043.
[20] J. Li, D. Oupicky, Effect of biodegradability on CXCR4 antagonism, transfection efficacy and antimetastatic activity of polymeric plerixafor, Biomaterials 35 (2014) 5572–5579, https://doi.org/10.1016/j.biomaterials.2014.03.047.
[21] B. García-Pinel, A. Ortega-Rodríguez, C. Porras-Alcalá, L. Cabeza, R. Contreras-Cáceres, R. Ortiz, A. Díaz, A. Moscoso, F. Sarabia, J. Prados, J.M. López-Romero, C. Melguizo, Magnetically active *p*NIPAM nanosystems as temperature-sensitive biocompatible structures for controlled drug delivery, Artif. Cells Nanomed, Biotechnol. 48 (2020) 1022–1055, https://doi.org/10.1080/21691401.2020.1773488.
[22] M. Doña-Flores, A. Ortega-Rodríguez, C. Alarcón-Fernández, J.M. López-Romero, R. Contreras-Cáceres, Effect of the cross-linking density on the gold core oxidation in hybrid core@shell Au@*p*NIPAM and Janus Au@*poly*-4VP systems, Colloids Surf. a. 584 (2020) 124014, https://doi.org/10.1016/j.colsurfa.2019.124014.
[23] R. Contreras-Cáceres, M.C. Leiva, R. Ortiz, A. Díaz, G. Perazzoli, M.A. Casado-Rodríguez, C. Melguizo, J.M. Baeyens, J.M. López-Romero, J. Prados, Paclitaxel-loaded hollow-*poly*(4-vinylpyridine) nanoparticles enhance drug chemotherapeutic efficacy in lung and breast cancer cell lines, Nano Res. 10 (2017) 856–875, https://doi.org/10.1007/s12274-016-1340-2.
[24] L.D. Martinenghi, R. Jønsson, T. Lund, H. Jenssen, Isolation, Purification, and Antimicrobial Characterization of Cannabidiolic Acid and Cannabidiol from Cannabis sativa L, Biomolecules 10 (2020) 900–915, https://doi.org/10.3390/biom10060900.
[25] J. Clara-Rahola, A. Moscoso, A.B. Ruiz-Muelle, M. Laurenti, P. Formanek, J. M. López-Romero, I. Fernández, J.F. Díaz, J. Rubio-Retama, A. Fery, R. Contreras-Cáceres, Au@*poly*-4VP core@shell pH-sensitive nanocomposites suitable for drug entrapment, J. Colloid Interface Sci. 514 (2018) 704–714, https://doi.org/10.1016/j.jcis.2017.12.072.
[26] X. Peng, J. Shen, Water-soluble copolymers. I. Biodegradability and functionality of *poly*[(sodium acrylate)-co-(4-vinylpyridine)], J. Appl. Polym. Sci. 71 (1999) 1953–57. 10.1002/(SICI)1097-4628(19990321)71:12<1953::AID-APP4>3.0.CO;2-1.
[27] K. Akamatsu, M. Shimada, T. Tsuruoka, H. Nawafune, S. Fujii, Y. Nakamura, Synthesis of pH-responsive nanocomposite microgels with size-controlled gold nanoparticles from ion-doped, lightly cross-linked *poly*(vinylpyridine), Langmuir 26 (2010) 1254–1259, https://doi.org/10.1021/la902450c.
[28] K.S. Kim, B. Vincent, pH and temperature-sensitive behaviors of *poly*(4-vinylpyridine-co-N-isopropylacrylamide), Microgels, Polym. J. 37 (2005) 565–570, https://doi.org/10.1295/polymj.37.565.
[29] F. Liu, A. Eisenberg, Preparation and pH triggered inversion of vesicles from *poly* (acrylic acid)-block-polystyrene-block-*poly*(4-vinyl pyridine), J. Am. Chem. Soc. 125 (2003) 15059–15064, https://doi.org/10.1021/ja038142r.
[30] L. Wu, U. Glebe, A. Böker, Synthesis of polystyrene and *poly*(4-vinylpyridine) mixed grafted silica nanoparticles via a combination of ATRP and CuI-catalyzed azide-alkyne Click chemistry, Macromol. Rapid Commun. 38 (2017) 160047, https://doi.org/10.1002/marc.201600475.
[31] S. Porcu, E. Tuveri, M. Palanca, C. Melis, I.M.L. Franca, J. Satta, D. Chiriu, C. M. Carbonaro, P. Cortis, A.D. Agostini, P.C. Ricci, Rapid in situ detection of THC and CBD in *Cannabis sativa* L. by 1064 nm Raman spectroscopy, Anal. Chem. 94 (2022) 10435–10442, https://doi.org/10.1021/acs.analchem.2c01629.
[32] L. Grifoni, G. Vanti, R. Donato, C. Sacco, A.R. Bilia, Promising nanocarriers to enhance solubility and bioavailability of cannabidiol for a plethora of therapeutic opportunities, Molecules 27 (2022) 6070–6092, https://doi.org/10.3390/molecules27186070.
[33] R. Ramer, K. Heinemann, J. Merkord, H. Rohde, A. Salamon, M. Linnebacher, COX-2 and PPAR-γ confer cannabidiol-induced apoptosis of human lung cancer cells, Mol. Cancer Ther. 12 (1) (2013) 69–82, https://doi.org/10.1158/1535-7163.MCT-12-0335.
[34] R. Ramer, K. Bublitz, N. Freimuth, J. Merkord, H. Rohde, M. Haustein, Cannabidiol inhibits lung cancer cell invasion and metastasis via intercellular adhesion molecule-1, FASEB J. 26 (4) (2011) 1535–1548, https://doi.org/10.1096/fj.11-198184.
[35] L. Milian, M. Mata, J. Alcacer, M. Oliver, M. Sancho-Tello, J.J. Martín, Cannabinoid receptor expression in non-small cell lung cancer. Effectiveness of tetrahydrocannabinol and cannabidiol inhibiting cell proliferation and epithelial-mesenchymal transition *in vitro*, PLoS ONE. 15 (2) (2020) e0228909, https://doi.org/10.1371/journal.pone.0228909.
[36] E.S. Seltzer, A.K. Watters, D. MacKenzie, L.M. Granat, D. Zhang, Cannabidiol (CBD) as a Promising Anti-Cancer Drug, Cancers 12 (11) (2020) 3203, https://doi.org/10.3390/cancers12113203.
[37] R. Ramer, J. Merkord, H. Rohde, B. Hinz, Cannabidiol inhibits cancer cell invasion via upregulation of tissue inhibitor of matrix metalloproteinases-1, Biochem. Pharmacol. 79 (7) (2010) 955–966, https://doi.org/10.1016/j.bcp.2009.11.007.
[38] M. Elbaz, M.W. Nasser, J. Ravi, N.A. Wani, D.K. Ahirwar, H. Zhao, Modulation of the tumor microenvironment and inhibition of EGF/EGFR pathway: novel anti-tumor mechanisms of cannabidiol in breast cancer, Mol. Oncol. 9 (4) (2015) 906–919, https://doi.org/10.1016/j.molonc.2014.12.010.
[39] F. Pellati, V. Borgonetti, V. Brighenti, M. Biagi, S. Benvenuti, L. Corsi, *Cannabis sativa* L. and nonpsychoactive cannabinoids: their chemistry and role against oxidative stress, inflammation and cancer, BioMed Res. Int. (2018) 1691428, https://doi.org/10.1155/2018/1691428.